Results in Physics 6 (2016) 1168–1174

Contents lists available at ScienceDirect

Results in Physics

journal homepage: www.journals.elsevier.com/results-in-physics

Unsteady boundary layer flow of Carreau fluid over a permeable stretching surface

Masood Khan, Muhammad Azam *

Department of Mathematics, Quaid-i-Azam University, Islamabad 44000, Pakistan

ARTICLE INFO

Article history:
Received 9 October 2016
Received in revised form 2 November 2016
Accepted 17 November 2016
Available online 25 November 2016

Keywords:
Unsteady boundary layer flow
Carreau fluid
Heat transfer
Numerical solutions

ABSTRACT

The main objective of the present work is to present numerical solutions of the unsteady two-dimensional boundary layer flow and heat transfer of an incompressible Carreau fluid over a permeable time dependent stretching sheet. Using suitable transformations, the time dependent partial differential equations are converted to non-linear ordinary differential equations. The numerical results of these non-linear ordinary differential equations with associated boundary conditions are determined by using the bvp4c function in MATLAB. The numerical results are investigated for the emerging parameters namely, the unsteadiness parameter A, mass transfer parameter S, Prandtl number Pr, power law index n and Weissenberg number We. It is important to state that both the momentum and thermal boundary layer thicknesses diminish with increasing values of the unsteadiness and mass transfer parameters. A comparison with the available literature in limiting cases is performed and found to be in good agreement.

Introduction

In recent years, the researchers have shown a keen interest in the study of shear driven flows involving the generalized Newtonian fluids due to their vast applications in engineering and scientific processes. The generalized Newtonian fluids are those in which viscosity of the fluid depends on the shear rate. The power law viscosity model is the most simplest generalized Newtonian fluid. However, the viscosity for very small and very large shear rates can not be predicted adequately by the power law viscosity model. Due to such limitations of the power law viscosity model, we consider another viscosity model from the class of the generalized Newtonian fluids named as Carreau rheological model. Carreau model overcomes the above said limitations of the power law model. This model possesses the ability of characterizing the rheology of different polymeric solutions such as 1% methylcellulose lylose in glycerol solution. Carreau model was first proposed by Carreau [1] in 1972. The constitutive law for the Carreau model can be written as $\boldsymbol{\tau} = -p\mathbf{I} + \mu(\dot{\gamma})\mathbf{A}_1$ with $\mu = \mu_\infty + (\mu_0 - \mu_\infty)[1 + (\Gamma\dot{\gamma})^2]^{\frac{n-1}{2}}$ where μ the apparent viscosity, p pressure, $\mathbf{I}$ identity tensor, $\mathbf{A}_1$ first rivlin-ericksen tensor defined by $\mathbf{A}_1 = (\text{grad}\mathbf{V}) + (\text{grad}\mathbf{V})^t$, μ_0 shows zero shear-rate viscosity and μ_∞ the infinite shear-rate viscosity. The shear rate $\dot{\gamma}$ is written as $\dot{\gamma} = \sqrt{\frac{1}{2}\Sigma_i\Sigma_j\dot{\gamma}_{ij}\dot{\gamma}_{ji}} = \sqrt{\frac{1}{2}\boldsymbol{\Pi}} = \sqrt{\frac{1}{2}tr(\mathbf{A}_1^2)}$ where $\boldsymbol{\Pi}$ is second invariant strain rate tensor. Here, we consider the case when $\mu_\infty = 0$ and thus $\boldsymbol{\tau} = -p\mathbf{I} + \mu_0[1 + (\Gamma\dot{\gamma})^2]^{\frac{n-1}{2}}\mathbf{A}_1$ where n is the power law index and Γ time material constant.

During the last few years, there has been a growing interest in studying the generalized Newtonian fluid model due to its wider acceptance in industrial and technological flows. To the best of our knowledge, the study of the Carreau fluid model has rarely been made in spite of its diverse applications. We have reported limited studies carried out on the flows of Carreau fluid. For instance, Hsu et al. [2] examined the electrophoresis of a sphere at an arbitrary position in a spherical cavity filled with Carreau fluid. Ali and Hayat [3] studied the peristaltic transport of Carreau fluid in an asymmetric channel. Tshehla [4] investigated the flow of Carreau fluid down an inclined free surface. Olajuwon [5] carried out the numerical study of heat and mass transfer of Carreau fluid with thermal radiation and thermal diffusion. Ashrafi and Mohamadali [6] investigated the numerical solutions of transient flows and heat transfer of shear thinning fluid. Recently, Khan et al. [7] studied the numerical solutions for MHD flow and heat transfer of Carreau fluid over stretching sheet with non-linear thermal radiation and convective boundary conditions. On the other hand, unsteady flow problems due to stretching surface have been investigated by various authors. For instance, Sharidan et al. [8] presented the similarly solutions for unsteady boundary layer flow and heat transfer of viscous fluid. Chamkha et al. [9] obtained

* Corresponding author.
E-mail address: mazam_25@yahoo.com (M. Azam).

http://dx.doi.org/10.1016/j.rinp.2016.11.035
2211-3797/

similarity solutions for transient heat and mass transfer in presence of suction. Mukhopadhyay and Gorla [10] discussed the effects of Maxwell parameter on heat transfer past a stretched sheet. Grubka and Bobba [11] and Chen [12] analyzed the effects of unsteadiness on heat transfer flows over stretching sheet. Hayat et al. [13] presented the series solutions for convective flow of Carreau nanofluid over a stretched surface. They observed that the impact of Brownian motion parameter and Lewis number on the local Nusselt and Sherwood numbers are qualitatively same. The study of MHD thixotropic nanomaterial in doubly stratified medium was reported by Hayat et al. [14]. They turned out that the thermal and concentration stratified parameters resulted in the diminishing of temperature and concentration profiles. The analysis on mixed convection flow of MHD micropolar fluid in the presence of convective surface condition was studied by Waqas et al. [15]. Impact of Cattaneo-Christov heat flux model for the stagnation point flow over a nonlinear stretched surface was investigated by Hayat et al. [16]. They pointed out that the temperature gradient increases when the thermal relaxation parameter is enhanced. Impact of variable thermal conductivity on the flow of generalized Burgers fluid with Cattaneo-Christov heat flux model was discussed by Waqas et al. [17]. They concluded that the fluid temperature predicted an inverse relationship with the thermal relaxation time. Due to vast applications of stretched flows in engineering and science, several studies over the stretched flows were reported by Hayat et al. [18–20].

Motivated by the above literature and applications, in the present work, the analysis is carried out to construct the numerical solutions of unsteady boundary layer flow and heat transfer of Carreau fluid over a permeable time dependent stretching sheet. It is an important to mention here that Carreau fluid is an important class of the generalized Newtonian fluid. To the best of authors knowledge, no attempt has been made so far to study the unsteady boundary layer flow and heat transfer of Carreau fluid over a permeable stretching surface. The aim of the present paper is to fill up the gap in existing literature.

Mathematical formulation

Consider a laminar two-dimensional unsteady boundary layer flow and heat transfer of an incompressible Carreau fluid in the region $y > 0$ over a time-dependent permeable stretching sheet. The physical model and coordinate system are shown in Fig. 1. The Cartesian coordinates x and y are chosen in such a way that x-axis is along the stretching sheet and y-axis is normal to it. The flow is generated due to the permeable stretching sheet by applying two equal and opposite forces along x-axis. It is assumed that the surface is moving with the velocity $U_w(x,t)$ and that the mass flux velocity is $V_w(t)$. It is also assumed that the temperature of the sheet is $T_w(x,t)$ and considered to be higher than the ambient temperature T_∞ $(T_w > T_\infty)$. The viscous dissipation effects are neglected in heat transfer process here. For the unsteady two-dimensional flow, the velocity and temperature fields are assumed to be of the form

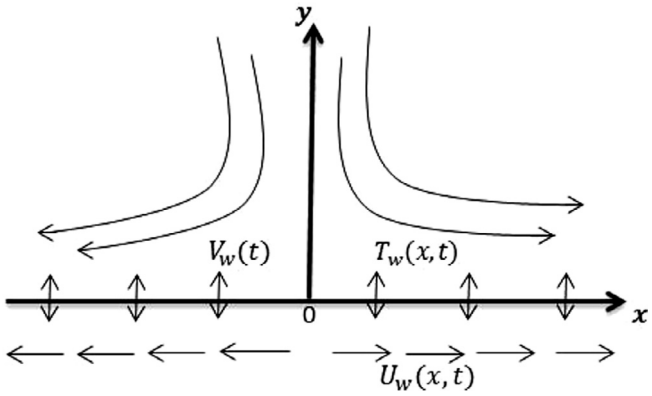

Fig. 1. Physical model and coordinate system.

$$\mathbf{V} = [u(x,y,t), v(x,y,t), 0], \quad T = T(x,y,t). \tag{1}$$

Under these assumptions, the basic boundary layer equations of the problem under consideration can be written as [21].

$$\frac{\partial u}{\partial x} + \frac{\partial v}{\partial y} = 0, \tag{2}$$

$$\frac{\partial u}{\partial t} + u\frac{\partial u}{\partial x} + v\frac{\partial u}{\partial y} = \nu\frac{\partial^2 u}{\partial y^2}\left[1 + \Gamma^2\left(\frac{\partial u}{\partial y}\right)^2\right]^{\frac{n-1}{2}} + \nu(n-1)\Gamma^2 \times \frac{\partial^2 u}{\partial y^2}\left(\frac{\partial u}{\partial y}\right)^2\left[1 + \Gamma^2\left(\frac{\partial u}{\partial y}\right)^2\right]^{\frac{n-3}{2}}, \tag{3}$$

$$\frac{\partial T}{\partial t} + u\frac{\partial T}{\partial x} + v\frac{\partial T}{\partial y} = \alpha\frac{\partial^2 T}{\partial y^2}, \tag{4}$$

along with the boundary conditions

$$u = U_w(x,t), \quad v = V_w(t), \; T = T_w(x,t) \quad at \quad y = 0, \tag{5}$$

$$u \to 0, \quad T \to T_\infty \quad as \quad y \to \infty. \tag{6}$$

where u and v represent the velocity components along the x- and y-directions, respectively, and t the time. Further, T and ν are the fluid temperature and kinematic viscosity, respectively, $\alpha\left(=\frac{k}{\rho C_p}\right)$ the thermal diffusivity with ρ fluid density, k thermal conductivity of the fluid and C_p the specific heat.

Further, we assumed that the stretching velocity $U_w(x,t)$, the surface temperature $T_w(x,t)$ and mass fluid velocity $V_w(t)$ are of the following form:

$$U_w(x,t) = \frac{ax}{1-ct}, \; T_w(x,t) = T_\infty + \frac{T_0 U_w x}{\nu(1-ct)^{\frac{1}{2}}}, \; V_w(t) = \frac{-V_0}{(1-ct)^{\frac{1}{2}}}, \tag{7}$$

where $ct < 1$ with a and c are positive constants having dimensions reciprocal of time. V_0 is a uniform suction/injection velocity ($V_0 > 0$ for suction and $V_0 < 0$ for injection). The effective stretching rate $\frac{1}{(1-ct)}$ increases or decreases with time since $c > 0$ or $c < 0$, respectively.

The following suitable transformations are used for the present case:

$$\eta = y\sqrt{\frac{U_w}{\nu x}}, \quad \Psi(x,y,t) = \sqrt{\nu U_w x} f(\eta), \quad \theta(\eta) = \frac{T - T_\infty}{T_w - T_\infty}, \tag{8}$$

where η is the new independent variable, Ψ represents stream function having the property $u = \frac{\partial \Psi}{\partial y}$, $v = -\frac{\partial \Psi}{\partial x}$.

By introducing the above transformations, the momentum and energy Eqs. (3) and (4), respectively, are transformed into following ordinary equations

$$\left\{1 + nWe^2(f'')^2\right\}\left\{1 + We^2(f'')^2\right\}^{\frac{n-3}{2}} f''' + ff'' - (f')^2 - A\left[f' + \frac{\eta}{2}f''\right] = 0, \tag{9}$$

$$\theta'' + \Pr(f\theta' - 2f'\theta) - \Pr\frac{A}{2}(\eta\theta' + 3\theta) = 0, \tag{10}$$

Table 1
Comparison of numerical results for $f''(0)$ for different values of the unsteadiness parameter A when $n=1, We=0$ and $S=0$ are fixed.

A	Sharidan et al. [8]	Chamkha et al. [9]	Mukhopadhyay et al. [10]	Present study
0.8	−1.261042	−1.261512	−1.261479	−1.261043
1.2	−1.377722	−1.378052	−1.377850	−1.377724

Table 2
Comparison of numerical results for $-\theta'(0)$ for different values of the Prandtl number Pr when $n=1, We=0, S=0$ and $A=0$ are fixed.

Pr	Grubka and Bobba [11]	Chen [12]	Present study
0.72	1.0885	1.08853	1.088915
1.00	1.3333	1.33334	1.333333
3.00	2.5097	2.50972	2.509698
10.0	4.7969	4.79686	4.796853

where prime shows differentiation with respect to η, $We\left(=\sqrt{\frac{a^3\Gamma^2x^2}{\nu(1-ct)^3}}\right)$ the local Weissenberg number, $\Pr\left(=\frac{\mu Cp}{k}\right)$ the Prandtl number and $A\left(=\frac{c}{a}\right)$ the unsteadiness parameter and the transformed boundary conditions are

$$f(0)=S,\ f'(0)=1,\ \theta(0)=1, \tag{11}$$

$$f'(\infty)\to 0, \theta(\infty)\to 0, \tag{12}$$

where $S\left(=\frac{V_0}{\sqrt{\nu a}}\right)$ is the constant mass transfer parameter with $S>0$ for suction and $S<0$ for injection. It should be noted that the results for viscous fluid can be achieved by putting $We=0$ in Eq. (9).

From the engineering point of view, the quantities of interest in this problem are the local skin friction coefficient C_{fx} and the local Nusselt number Nu_x, which are given by

$$C_{fx}=\frac{\tau_w}{\rho U_w^2}, \quad Nu_x=\frac{xq_w}{k(T_w-T_\infty)}, \tag{13}$$

where the wall shear stress τ_w and the wall heat flux q_w are defined as

$$\tau_w=\left(\mu_0\frac{\partial u}{\partial y}\left[1+\Gamma^2\left(\frac{\partial u}{\partial y}\right)^2\right]^{\frac{n-1}{2}}\right)_{y=0}, \quad q_w=-k\left(\frac{\partial T}{\partial y}\right)_{y=0}, \tag{14}$$

with μ_0 as zero shear rate viscosity.

Thus substituting Eq. (8) into Eq. (14) and using Eq. (13) the following expressions can be attained

$$\mathrm{Re}^{1/2}C_{fx}=f''(0)\left[1+We^2(f''(0))^2\right]^{\frac{n-1}{2}} \quad \mathrm{Re}^{-1/2}Nu_x=-\theta'(0), \tag{15}$$

where $\mathrm{Re}_x\ \left(=\frac{xU_w}{\nu}\right)$ is the local Reynolds number.

Discrete scheme and solution methodology

The non-linear ordinary differential Eqs. (9) and (10) subject to the boundary conditions (11) and (12) are solved numerically by utilizing numerical technique known as bvp4c function in MATLAB. This method is based on the collocation method for solving boundary value problem of the form

$$y'=f(x,y,\mathbf{p}), \quad a\leqslant x\leqslant b, \tag{16}$$

with the general nonlinear, two-point boundary conditions

Table 3
Numerical values of the local skin friction $Re^{1/2}C_{fx}$ and the local Nusselt number $\mathrm{Re}^{-1/2}Nu_x$ for various A, S, We and n when $\Pr=0.72$ are fixed.

Parameters			$\mathrm{Re}^{1/2}C_{fx}$		$\mathrm{Re}^{-1/2}Nu_x$	
A	S	We	$n=0.5$	$n=1.5$	$n=0.5$	$n=1.5$
0	0.1	1	−0.984502	−1.105730	1.095643	1.135326
0.5	–	–	−1.123568	−1.287783	1.299407	1.337392
1	–	–	−1.246418	−1.459715	1.467672	1.506087
2	–	–	−1.449686	−1.767831	1.753517	1.792850
1	0.1	–	−1.246418	−1.459715	1.467672	1.506087
–	0.3	–	−1.335645	−1.565328	1.528805	1.574201
–	0.5	–	−1.432546	−1.678373	1.592750	1.645860
–	0.7	–	−1.537409	−1.798792	1.659714	1.721167
–	0.3	1	−1.335645	−1.565328	1.528805	1.574201
–	–	3	−1.057255	−1.778164	1.460781	1.602252
–	–	5	−0.924956	−1.924107	1.422661	1.616516
–	–	7	−0.845930	−2.034999	1.397207	1.625560

Table 4
Numerical values of the local Nusselt number $\mathrm{Re}^{-1/2}Nu_x$ for various $\Pr, A, S$ and n when $We=3$ is fixed.

Parameters			$\mathrm{Re}^{-1/2}Nu_x$		
Pr	A	S	$n=0.5$	$n=1$	$n=1.5$
0.72	0.4	0.3	1.242221	1.349189	1.402305
1	–	–	1.532060	1.655670	1.713346
3	–	–	3.095507	3.271185	3.338009
7	–	–	5.382384	5.586108	5.654414
1	0	–	1.336608	1.475306	1.542443
–	0.8	–	1.699923	1.814883	1.867066
–	1.2	–	1.851349	1.959863	2.008210
–	2	–	2.120781	2.219770	2.262867
–	0.8	0	1.583452	1.672845	1.715929
–	–	0.5	1.783838	1.916890	1.975349
–	–	1	2.021771	2.198410	2.272115
–	–	1.5	2.308189	2.517657	2.604050

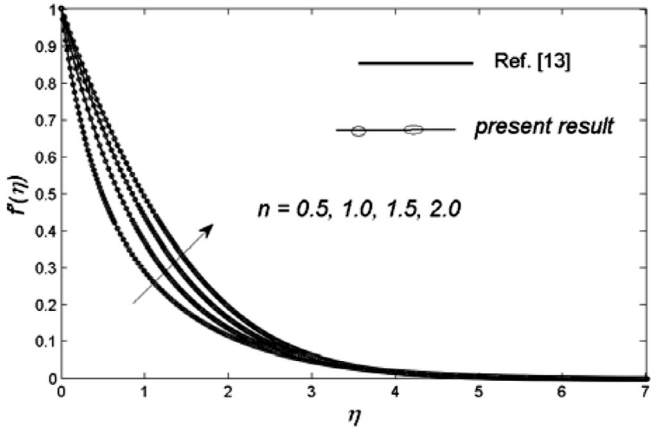

Fig. 2. A comparison of velocity profiles $f'(\eta)$ for different values of the power law index n when $We = 3$ and $S = A = 0$ are fixed.

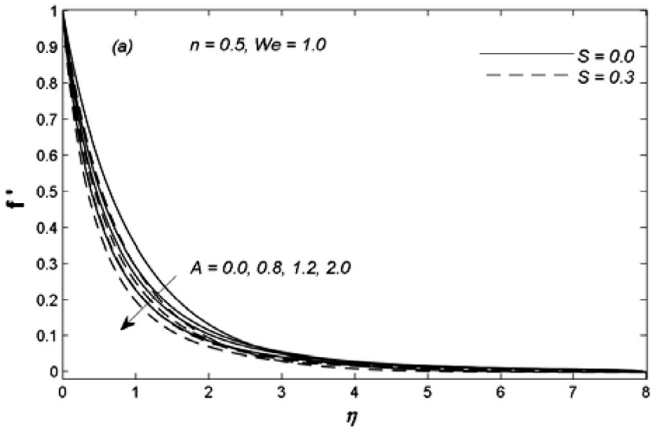

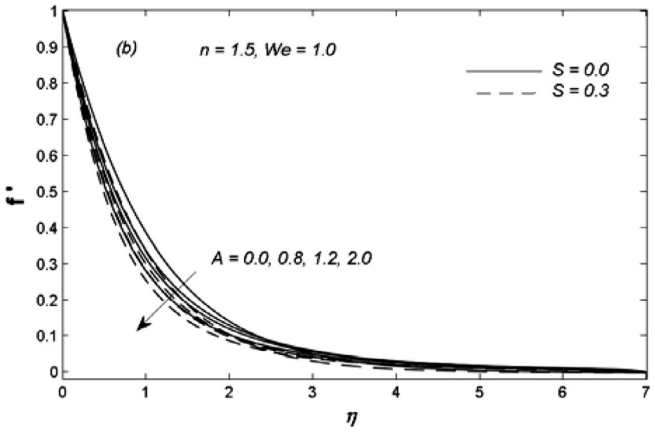

Fig. 3. Velocity profiles $f'(\eta)$ for different values of the unsteadiness parameter A.

$$g(y(a), y(b), \mathbf{p}) = 0, \tag{17}$$

where $\mathbf{p}$ is a vector of unknown parameters. The approximate solution $\mathbf{S}(x)$ is a continuous function which is a cubic polynomial on each subinterval $[x_n, x_{n+1}]$ of a mesh $a = x_0 < x_1 < x_2 < \ldots\ldots < x_n = b$ satisfying the boundary conditions

$$g(\mathbf{S}(a), \mathbf{S}(b)) = 0. \tag{18}$$

This solution also satisfies the differential equation system at mid point and end points of each subinterval

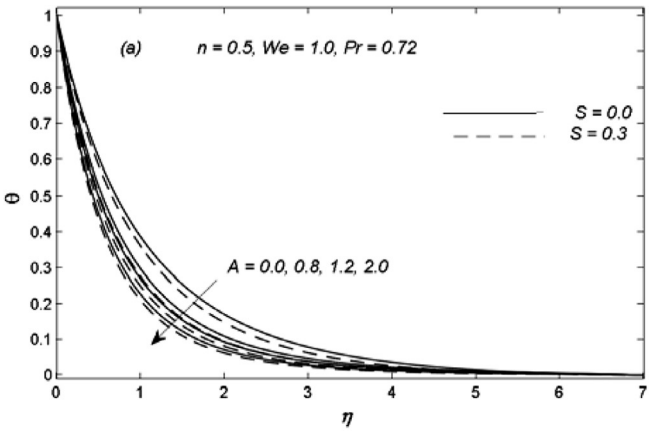

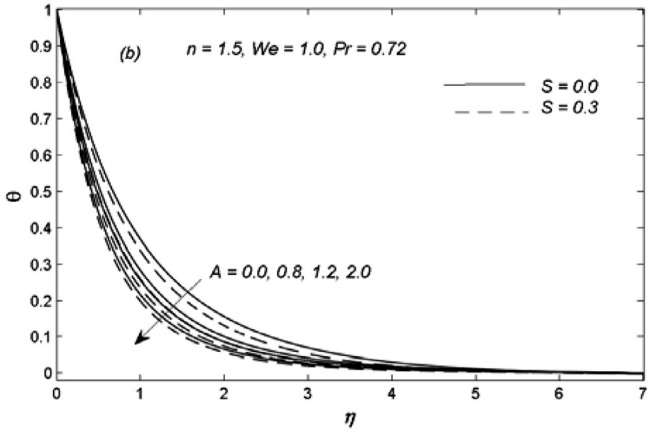

Fig. 4. Temperature profiles $\theta(\eta)$ for different values of the unsteadiness parameter A.

$$\mathbf{S}'(x_n) = f(x_n, S(x_n)), \tag{19}$$

$$\mathbf{S}'((x_n + x_{n+1})/2) = f((x_n + x_{n+1})/2, \quad S((x_n + x_{n+1})/2)), \tag{20}$$

$$\mathbf{S}'(x_{n+1}) = f(x_{n+1}, \mathbf{S}(x_{n+1})). \tag{21}$$

The above conditions conclude in a system of nonlinear algebraic equations for the coefficients defining $\mathbf{S}$. In comparison to shooting method, the solution $y(x)$ is approximated over the whole interval $[a, b]$ and the subsidary conditions are taken into account every time. The nonlinear algebraic system is solved iteratively by linearization. It is important to mentioned that this approach relies upon the linear equation solver of the MATLAB rather than its initial value problem codes. The basic method of bvp4c is the Simpson's method which can be seen in a number of codes. It can be seen that with the modest consideration, $\mathbf{S}(x)$ is the fourth order approximation to an isolated solution $y(x)$ which implies $\|\mathbf{y}(x) - \mathbf{S}(x)\| \leqslant Ch^4$ where C is the constant and h is the highest of the step sizes $h_n = x_{n+1} - x_n$. After the computation of $\mathbf{S}(x)$ on a mesh with the help of bvp4c, it can be solved at any x or a set of x in the interval $[a, b]$. The boundary value problem codes demand users to provide a guess for the required solution. The guess includes a guess for an initial mesh that depicts the behavior of the required solution. The codes then use the mesh so as to obtain a required solution with the modest mesh points. The residual $\mathbf{r}(x)$ for such an approximation in the ordinary differential equation systems is defined as

$$\mathbf{r}(x) = \mathbf{S}'(x) - \mathbf{f}(x, \mathbf{S}(x)). \tag{22}$$

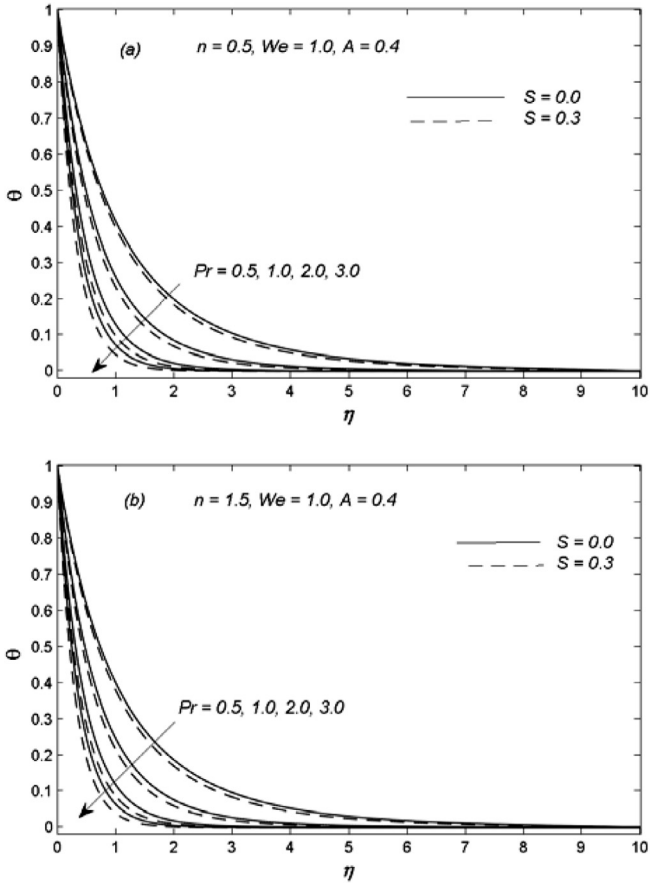

Fig. 5. Temperature profiles $\theta(\eta)$ for different values of the Prandtl number Pr.

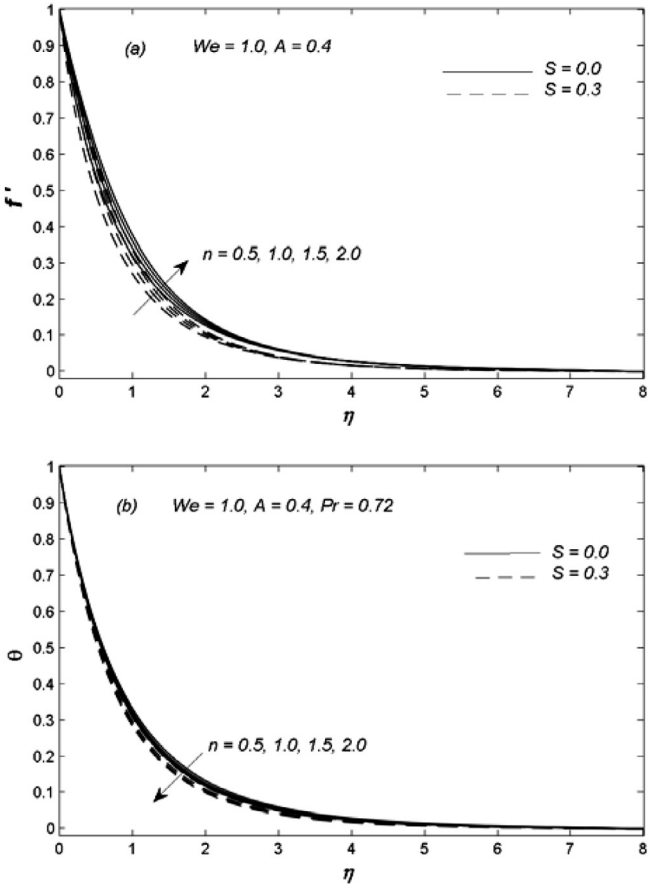

Fig. 6. Velocity profiles $f'(\eta)$ and temperature profiles $\theta(\eta)$ for various power law index n.

It implies that $\mathbf{S}(x)$ is the exact solution of the perturbed ordinary differential equations.

$$\mathbf{S}'(x) = \mathbf{f}(x, \mathbf{S}(x)) + \mathbf{r}(x). \tag{23}$$

Similarly, $\mathbf{g}(S(a), S(b))$ is the residual in the boundary condition. If the residual is small then it means $\mathbf{S}(x)$ is close to $y(x)$. It is important to state here that depends on algorithms that are plausible even though the initial mesh is very poor, yet furnish the correct results as $h \to 0$ [22].

Results and discussion

The non-linear differential Eqs. (9) and (10) with the associated boundary conditions (11) and (12) are solved numerically by using the numerical technique namely bvp4c function in MATLAB. The numerical results are obtained for different values of the emerging parameters namely, unsteadiness parameter A, power law index n, Prandtl number Pr, local Weissenberg number We, and mass transfer parameter S. The impact of these parameters on the velocity and temperature profiles are shown graphically. The numerical values of the local skin-friction coefficient $Re^{1/2}C_{fx}$ and the local Nusselt number $\mathrm{Re}^{-1/2}Nu_x$ are also tabulated in Table 3 for various values of emerging parameters. Furthermore, the numerical calculations for the Nusselt number $-\theta'(0)$ are presented in Table 4 for various values of physical parameters. In order to check the accuracy of the present computed results with available published data, a comparison is performed between current computed results and available literature in limiting cases.

Table 1 shows a comparison of the numerical results of the skin-friction coefficient $f''(0)$ for different values of the unsteadiness parameter A when $n = 1, We = 0$ and $S = 0$ are fixed with published results of Sharidan et al. [8], Chamkha et al. [9] and Mukhopadhyay et al. [10]. On the evident of Table 1, the results are found in outstanding agreement. Table 2 also represents a comparison of the present numerical results of the Nusselt number $-\theta'(0)$ for different values of Prandtl number Pr when $n = 1, We = 0, S = 0$ and $A = 0$ are fixed with available published results of Grubka and Bobba [11] and Chen [12]. From Table 2, it is clear that the results are found in excellent agreement. The variations of various values of the unsteadiness parameter A, mass transfer parameter S and Weissenberg number We on the local skin friction coefficient $Re^{1/2}C_{fx}$ and the local Nusselt number $\mathrm{Re}^{-1/2}Nu_x$ for both shear thinning $(0 < n < 1)$ and shear thickening $(n > 1)$ fluids are depicted in Table 3. It is obvious that by increasing the values of the unsteadiness parameter A and mass transfer parameter S, the magnitude of the local skin friction coefficient $Re^{1/2}C_{fx}$ increases in both shear thinning and shear thickening fluids. It is interesting to note that by increasing the values of the Weissenberg number We, the magnitude of the local skin friction coefficient decreases for the shear thinning fluid and increases for shear thickening fluid. From Table 3, it can be seen that the local Nusselt number is an increasing function of the unsteadiness parameter A and mass transfer parameter S both for shear thinning and shear thickening fluids. However, on incrementing the values of the Weissenberg number We, the local Nusselt number $\mathrm{Re}^{-1/2}Nu_x$ decreases in shear thinning fluid but increases in shear thickening fluid. The numerical results of the local Nusselt number $\mathrm{Re}^{-1/2}Nu_x$ for several values of the Prandtl number Pr, unsteadiness parameter A and mass transfer parameter S are tabulated in Table 4 both for shear thinning and shear thickening fluids. From Table 1, it

is depicted that the local Nusselt number $\mathrm{Re}^{-1/2}Nu_x$ is an increasing function of the Prandtl number Pr, unsteadiness parameter A and mass transfer parameter S both for shear thinning fluid as well as shear thickening fluid. Fig. 2 is constructed to represent the comparison of velocity profiles between Khan and Hashim [21] and the present study. On the basis of this Fig., it can be seen that the result are in good agreement.

The behavior of unsteadiness parameter A on the velocity field $f'(\eta)$ in the presence and absence of mass transfer parameter S is displayed in Fig. 3(a) and (b) for both shear thinning and shear thickening fluids. It is observed that when the unsteadiness parameter A increases, the velocity field $f'(\eta)$ and momentum boundary layer thickness decrease in both the shear thinning and shear thickening fluids. However, it is observed that the momentum boundary layer thickness is larger in case of the shear thickening fluid as compared to the shear thinning fluid. The temperature field $\theta(\eta)$ for different values of the unsteadiness parameter A is shown graphically in Fig. 4(a) and (b). From these Figs., it is noted that the impact of increasing the values of unsteadiness parameter A is to diminish the temperature field $\theta(\eta)$ and thermal boundary layer thickness. Physically, when unsteadiness enhances the sheet looses more heat due to which temperature diminishes. The behavior of temperature field $\theta(\eta)$ for different values of the Prandtl number Pr is displayed in Fig. 5(a) and (b). From these Figs., it is noticed that an increase in the values of Prandtl number Pr results in a decrease in temperature field $\theta(\eta)$ and thermal boundary layer thickness both in shear thinning and shear thickening fluids. This is because of the fact that the fluid with higher Prandtl number possesses low thermal conductivity and consequently reduces the conduction and the thermal boundary layer thickness. Fig. 6(a) and (b) elucidate the influence of the power law index n on the velocity profiles $f'(\eta)$ and temperature profiles $\theta(\eta)$, respectively. These Figs. put in conformation that the velocity field $f'(\eta)$ is an increasing function of the power law index n while temperature field $\theta(\eta)$ is a decreasing function of it. Fig. 7(a) and (b) are plotted to illustrate the influence of the local Weissenberg number We on the velocity field $f'(\eta)$ and the temperature field $\theta(\eta)$ for both cases of shear thinning and shear thickening fluids. From these Figs., it is noticed that the velocity field $f'(\eta)$ decreases by uplifting the Weissenberg number We in shear thinning fluid and opposite behavior has been seen in shear thickening fluid. As far as the temperature field is concerned, it increases by increasing the values of the Weissenberg number We in shear thinning fluid. However, quite the opposite behavior is noticed for the shear thickening fluid. By the definition of the Weissenberg number, it is the ratio of the relaxation time of the fluid and a specific process time. It improves the thickness of the fluid and that is why the velocity of the fluid diminishes. High Weissenberg flows means long relaxation time in which the velocity of the fluid vanishes at the wall and away from the wall the particles move long distances within one relaxation time and the particles close the wall move short distance. Fig. 8(a) and (b) are drawn to analyze the effects of mass transfer parameter S on velocity field $f'(\eta)$ and temperature field $\theta(\eta)$ for both cases of shear thinning and shear thickening fluids. These figures indicate that the velocity and temperature decrease by increasing the values of mass transfer parameter S. It is important to mention here that mass transfer reduces the momentum boundary layer as well as thermal boundary layer thicknesses.

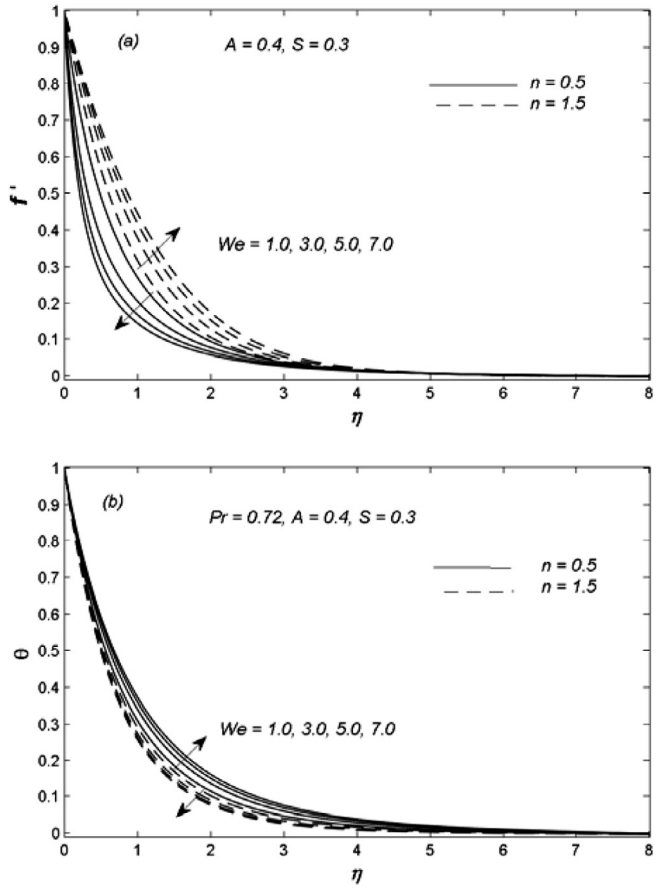

Fig. 7. Velocity profiles $f'(\eta)$ and temperature profiles $\theta(\eta)$ for various Weissenberg number We.

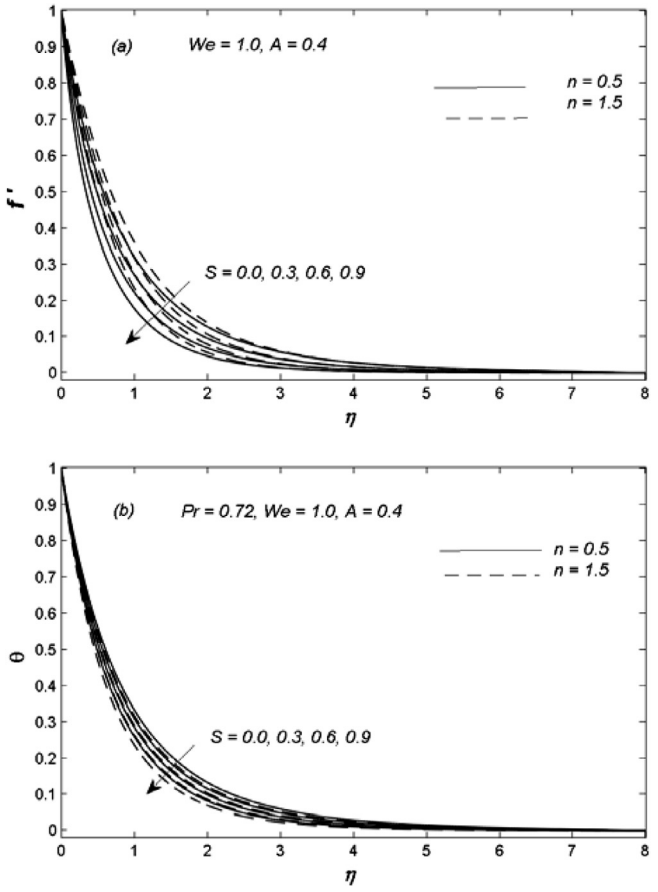

Fig. 8. Velocity profiles $f'(\eta)$ and temperature profiles $\theta(\eta)$ for various mass transfer parameter S.

Conclusions

In the present work, the bvp4c function in MATLAB was used to present the numerical solutions for the unsteady two-dimensional boundary layer flow and heat transfer of an incompressible Carreau fluid over a permeable time dependent stretching sheet. The numerical results were compared with avaible published data and have been found in an excellent agreement. The centre of attention of the present investigation was to explore the effects of the emerging parameters namely, the unsteadiness parameter A, mass transfer parameter S, power law index n, local Weissenberg number We and Prandtl number Pr on the dimensionless velocity profiles $f'(\eta)$, temperature profiles $\theta(\eta)$, local skin friction coefficient $\mathrm{Re}^{1/2}C_{fx}$ and local Nusselt number $\mathrm{Re}^{-1/2}Nu_x$. The important results are summarized as:

- The dimensionless velocity profiles $f'(\eta)$ as well as temperature profiles $\theta(\eta)$ were decreased with an increment in the unsteadiness parameter A and mass transfer parameter S for both shear thinning $(0 < n < 1)$ and shear thickening $(n > 1)$ fluids.
- The momentum boundary layer thickness and thermal boundary layer thickness were decreasing function of the unsteadiness parameter A and the mass transfer parameter S for both shear thinning $(0 < n < 1)$ and shear thickening $(n > 1)$ fluids.
- An increase in the Weissenberg number We resulted in a decrement in the fluid velocity $f'(\eta)$ in shear thinning fluid and opposite effects in shear thickening fluid are as seen. However, quite the opposite was true for temperature field.
- On increasing the values of the mass transfer parameter S, the momentum and thermal boundary layer thicknesses were decreased. However, the thermal boundary layer thickness was thicker in shear thinning fluid when compared with the shear thickening fluid.
- The magnitude of the local skin friction coefficient was increased with an increment in the unsteadiness parameter A and mass transfer parameter S both for shear thinning and shear thickening fluids.
- The local Nusselt number was increased with an increase in unsteadiness parameter A and mass transfer parameter S both for shear thinning and shear thickening fluids.

The present analysis can be extended for gyrotactic microorganisms and homogeneous-heterogenous reactions. The analysis can also be extended for the case of variable thermal conductivity in the presence of magnetic field etc.

Acknowledgment

We would like to thank the anonymous reviewers for the careful reading and essential comments.

References

[1] Carreau PJ. Rheological equations from molecular network theories. Trans Soc Rheol 1972;116:99–127.
[2] Hsu P, Hung SH, Yu H. Electrophoresis of a sphere at an arbitrary position in a spherical cavity filled with Carreau fluid. J Colloid Interface Sci 2004;280:256–63.
[3] Ali N, Hayat T. Peristaltic motion of a Carreau fluid in an asymmetric channel. Appl Math Comput 2007;193:535–52.
[4] Tshehla MS. The flow of Carreau fluid down an inclined with a free surface. Int J Phys Sci 2011;6:3896–910.
[5] Olajuwon BI. Convection heat and mass transfer in a hydromgnetic Carreau fluid past a vertical porous plate in presence of thermal radiation and thermal diffusion. Therm Sci 2011;15(2):241–52.
[6] Ashrafi N, Mohamadali M. Transient flow and heat transfer of pseudoplastic fluids. Appl Math Comput 2014;228:153–61.
[7] Khan M, Hashim, Hussain M, Azam M. Magnetohydrodynamic flow of Carreau fluid over a convectively heated surface in the presence of non-linear radiation. J Magn Magn Mater 2016;412:63–8.
[8] Sharidan S, Mahmood T, Pop I. Similarity solutions for the unsteady boundary layer flow and heat transfer due to a stretching sheet. Int J Appl Mech Eng 2006;11(3):647–54.
[9] Chamkha AJ, Aly AM, Mansour MA. Similarity solution for unsteady heat and mass transfer from a stretching surface embedded in a porous medium with suction/injection and chemical reaction effects. Chem Eng Commun 2010;197:846–58.
[10] Mukhopadhyay S, Gorla RSR. Unsteady MHD boundary layer flow of an upper convected Maxwell fluid past a stretching sheet with first order constructive/destructive chemical reaction. J Naval Archit Mar Eng 2012;9:123–33.
[11] Grubka LJ, Bobba KM. Heat transfer characteristics of a continuous stretching surface with variable temperature. ASME J Heat Transf 1985;107:248–50.
[12] Chen CH. Laminar mixed convection adjacent to vertical continuously stretching sheets. Heat Mass Transf 1998;33:471–6.
[13] Hayat T, Waqas M, Shehzad SA, Alsaedi A. Stretched flow of Carreau nanofluid with convective boundary condition. Pramana J. Phys. 2016;86:3–17.
[14] Hayat T, Waqas M, Khan MI, Alsaedi A. Analysis of thixotropic nanomaterial in a doubly stratified medium considering magnetic field effects. Int J Heat Mass Transf 2016;102:1123–9.
[15] Waqas M, Farooq M, Khan MI, Alsaedi A, Hayat T, Yasmeen T. Magnetohydrodynamic (MHD) mixed convection flow of micropolar liquid due to nonlinear stretched sheet with convective condition. Int J Heat Mass Transf 2016;102:766–72.
[16] Hayat T, Zubair M, Ayub M, Waqas M, Alsaedi A. Stagnation point flow towards nonlinear stretching surface with Cattaneo–Christov heat flux. Eur Phys J Plus 2016;131:355.
[17] Waqas M, Hayat T, Farooq M, Shehzad SA, Alsaedi A. Cattaneo–Christov heat flux model for flow of variable thermal conductivity generalized Burgers fluid. J Mol Liq 2016;220:642–8.
[18] Hayat T, Khan MI, Waqas M, Alsaedi A, Yasmeen T. Diffusion of chemically reactive species in third grade flow over an exponentially stretching sheet considering magnetic field effects. Chin J Chem Eng 2016. http://dx.doi.org/10.1016/j.cjche.2016.06.008.
[19] Hayat T, Waqas M, Shehzad SA, Alsaedi A. A model of solar radiation and Joule heating in magnetohydrodynamic (MHD) convective flow of thixotropic nanofluid. J Mol Liq 2016;215:704–10.
[20] Hayat T, Bahir G, Waqas M, Alsaedi A. MHD flow of Jeffrey liquid due to a nonlinear radially stretched sheet in presence of Newtonian heating. Res Phys 2016;6:817–23.
[21] Khan M, Hashim. Boundary layer flow and heat transfer to Carreau fluid over a nonlinear stretching sheet. AIP Adv 2015;5. 107203.
[22] Shampine, Kierzenka LF. Solving boundary value problems for ordinary differential equations in MATLAB with bvp4c, Tutorial Notes; 2000.